Structural and Optical Properties of Sno2:Mno2 Nanostructure Thin Films

Khalil Taha Jadaan, Faisal Ghazi Hammoodi, Muhammad Hameed Al-Timimi

Department of Physics, College of Science, University of Diyala, Iraq. nday@naver.com

In this research, the deposition of tin oxide (SnO2) films doped with manganese oxide (MnO2) at (350 ºC) on glass substrates was studied using chemical spray pyrolysis. The structural, optical, and surface topographic properties of the films were investigated. The results revealed that the prepared films were polycrystalline with a tetragonal crystal structure. The optical measurements show that the transmittance increases with increasing wavelength for all the prepared films, while the absorbance and reflectance decrease. As for the absorption coefficient, refractive index, and energy gap increase with increasing photon energy, where the energy gap value reaches around (3.0-3.5) eV. The extinction coefficient, real and imaginary parts of the dielectric constant decrease with increasing incident photon energy. The surface topographic study showed that all prepared films' roughness values and root-mean-square roughness increased.

Keywords: SnO2, MnO2 , Thin Films , XRD, AFM, optical Properties.

1. Introduction

Transparent tin oxide is a chemical material known as tin oxide or tin dioxide (SnO2)[1] . It is an important material with diverse applications in the fields of electronics, energy, and industry, and its unique properties have made it a subject of wide interest in research and development. It is widely used in the electronics industry as a transparent, electrically conductive material, such as in touchscreens and solar panels. It is also used in applications for transparent and scratch-resistant coatings [2], as well as in lithium-ion batteries [3]. It is used as a catalytic material in many chemical reactions [4], and it is used as a sensing material for gases and humidity due to its variable electrical properties [5]. It is also used in automotive glass and optical crystals [6]. Transparent manganese oxide is a chemical compound with the formula (MnO2) [7]. Manganese oxide or manganese dioxide is a compound composed of two oxygen atoms bonded to one manganese atom [8]. It appears as solid brown crystals and is a semi-conductive material for electricity and heat [9]. Transparent manganese oxide is used in

various applications [10], including the production of metallic manganese [11], in dry batteries[12], as an oxidizing agent in the chemical industry, and as a catalyst in some industrial processes[13]. Thin films are thin layers of materials with thicknesses typically ranging from a few nanometers to a few micrometers [14] . These films are characterized by their homogeneity and regularity in terms of crystalline and chemical structure at the atomic and molecular level [15].Thin films are important materials in various fields, including electronics [16], solar energy[17], sensors [18] , electrochemical devices[19] , protective coatings [20], biotechnology [21], and many others. The preparation of SnO2:MnO2 thin films is typically achieved using techniques such as vacuum evaporation [22], thermal combustion [23], chemical deposition [24], thermal crystallization [25], and electrochemical deposition[26]. Chemical spray pyrolysis (CSP) is a versatile thin-film deposition technique used in materials science and engineering [27] . It is a modified form of the conventional spray pyrolysis method that involves the synthesis of thin films or coatings by the decomposition of precursor solutions through pyrolysis [28].The process begins with the preparation of a precursor solution that contains the desired chemical components for the film. This solution is typically prepared by dissolving metal salts, organic compounds, or other precursors in a suitable solvent. The precursor solution is then atomized into fine droplets using a spray nozzle[29,30].

The current study aims to prepare Nanoscale films of pure tin oxide doped with manganese dioxide to study the effect of manganese dioxide doping on the structural, optical, and electrical properties of the prepared films. This is done for their potential use in practical applications in the field of solar cell manufacturing and sensors.

2. Experimental

The chemical spray pyrolysis (CSP) technique has been used to manufacture thin films of tin dioxide doped with manganese oxide (SnO2: MnO2). The prepared thin films are grown on clean glass substrates with dimensions of (2.5x2.5) cm at (350 ºC). The crystalline structure of the prepared films is determined using a (Shimadzu XRD-6000 Powder) X-ray diffract meter with (Cu Kα) radiation within the available wavelength and range at the Technological University, and To study the effect of manganese oxide (MnO2) doping on the (SnO2) films and compare the results with established values in standard cards, the absorbance and transmittance spectra were measured using a (Shimadzu UV-Visible 1800 Spectrophotometer) equipped in the research laboratory at the College of Sciences, Diyala University.

3. Results and discussion

X-Ray Diffraction

The X-ray diffraction (XRD) exam have been done for prepared nanomaterials in order to investigate the crystal structure and the crystalline size using x-ray diffractometer (Shimadzu-6000), with wavelength ($^{o}\lambda$=1.54060A) and voltage (40 KV). Figure 1 presents the experimental XRD patterns of prepared nanomaterials. The obtained characteristic peaks at (2Θ = 26.58^{o}, 33.87^{o}, 37.95^{o}, 51.76^{o}, 54.75^{o}, 61.87 ^{o}, 64.72^{o}) of the crystalline planes (110), (011), (020), (121) (220), (130) and (031) revealed the formation of Cassiterite tetragonal

SnO2 structure, space group (P42/mnm no. 136), with lattice parameters (a = b = 4.7380 A^{o} and c = 3.1870 A^{o}) and ($\alpha = \beta = \gamma = 90^{o}$), which well agreed with the standard data (JCPDS 98-000-9163) [31], As presented in figure 1(a). The XRD results demonstrated the pure crystalline structure of the synthesized SnO2 nanoparticles, there are no other peaks detected in the experimental XRD pattern. After doping with MnO2, the XRD patterns indicated that the SnO2 crystal structure doesn't affected at all MnO2 ratios (2, 4, 6 and 8 wt. %) as shown in figure 1(b, c, d, e), which can be described as the Mn ions were inserted within the crystalline lattice of SnO2. The obtained XRD patterns revealed that the peaks width of pure SnO2 increased, while the peaks intensity decreased after doping with Mn ions, where the added Mn ions led to decrease the crystalline growth of SnO2, as a result to the bigger diameter of Sn ions (0.071 nm) compared to the Mn ions (0.067nm)[32,33] The crystalline size of pure SnO2 and doped at different ratio (2, 4, 6 and 8 wt. %) of Mn ions calculated depending on the highest XRD peak using Debye Scherrer's equation, to be (42.53 nm), (39.45 nm), (23.16 nm), (21.75 nm), (18.22 nm) respectively, The obtained results demonstrated a significant decreasing in the crystalline size with the doping ratio.

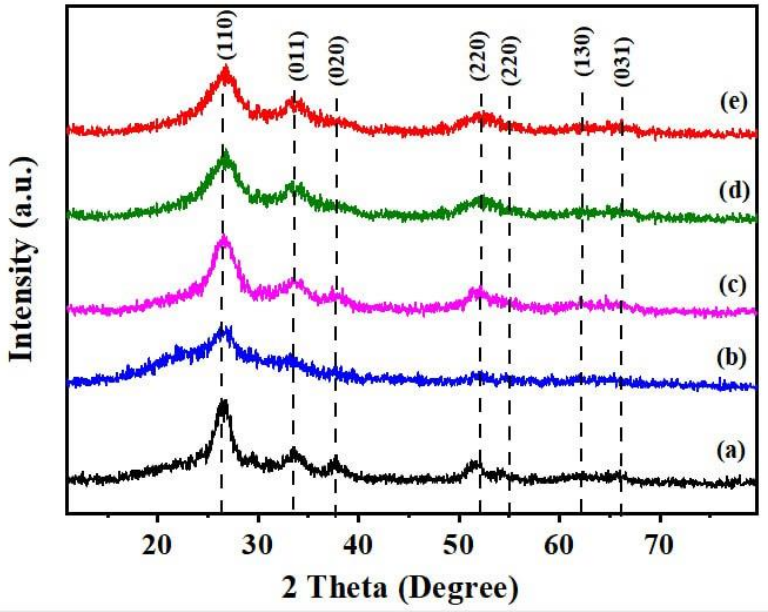

Fig.)1 (: XRD for (a) pure SnO2, (b) SnO2 /MnO2 (2%) (c) SnO2 /MnO2 (4%) (d) SnO2 /MnO2 (6%) (e) SnO2 /MnO2 (8%).

Atomic Force Microscopy (AFM)

The figures (1-a), (2-b), and (2-c) display the results of Atomic Force Microscopy (AFM) studies conducted on thin films of (SnO2) and (MnO2) prepared with different doping ratios. AFM is a high-resolution imaging and analysis technique used to examine the surfaces of films and provide precise measurements of particle size distribution and surface roughness. From Table (1), it is observed that the average roughness values and the root mean square roughness values increase for all the prepared films. This is attributed to the fact that the doping particles of (MnO2) occupy intermediate positions within the crystal lattice [34]. Moreover, positive

values of surface tilt, which are used to measure the extent of external coordination of the surface, indicate that the distribution of heights is higher than the depressions. Conversely, negative values indicate that the depressions are higher than the heights. In both cases, the distribution is asymmetric, and for a symmetric distribution, the surface tilt should be zero. When the surface gradient exceeds (3) , the surface possesses more peaks than depressions, while for values below (3), the surface appears flat. The profile takes the form of an arch for values equal to (3) [35].

Table (1): Some topographical parameters of (SnO2:MnO2) thin films.

Samples	**Average Roughnes Sa (nm)**	**RMS (nm)**	**Particle Size (nm)**	**Surface Sleekness (Ssk) (nm)**	**Surface Kurtosis (SKu) (nm)**	**Maximum Height Sz (nm)**
SnO_2	14.24	17.11	130	-0.4239	2.654	125.1
$(SnO_2)_{0.98}(MnO_2)_{0.2}$	39.44	49.36	204	0.2593	3.264	334.1
$(SnO_2)_{0.92}(MnO_2)_{0.8}$	15.62	19.68	131	0.07461	2.927	132.0

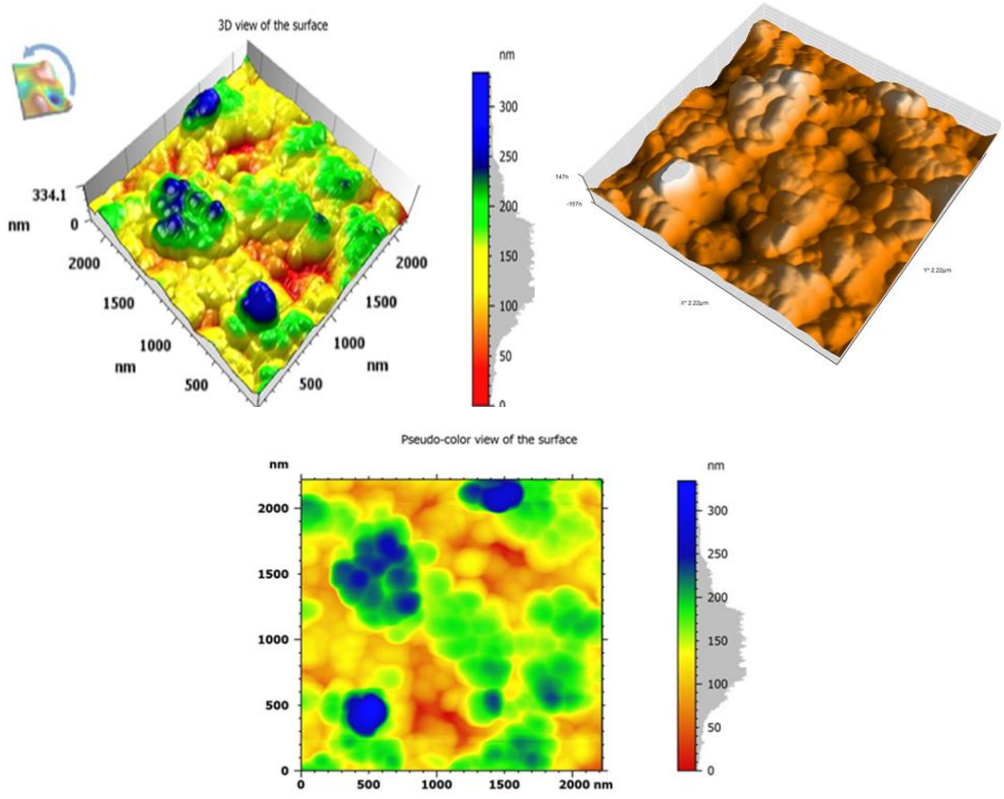

Fig.(2-a): AFM Images of pure SnO_2 thin film.

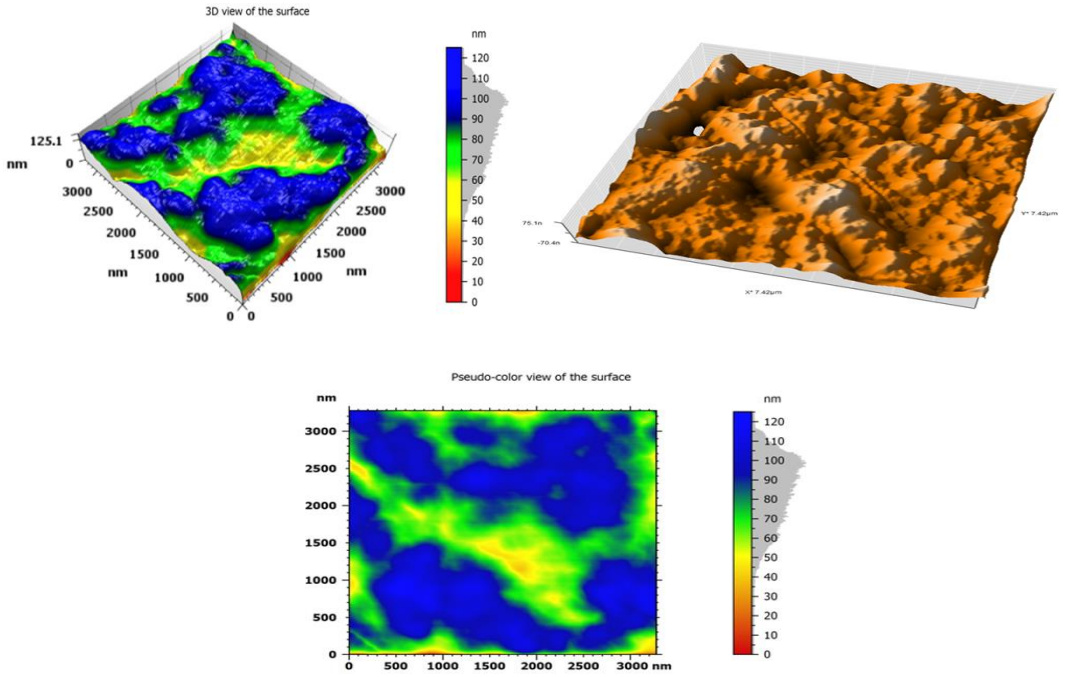

Fig.(2-b): AFM Images of $(SnO_2)_{0.98}(MnO_2)_{0.2}$thin film

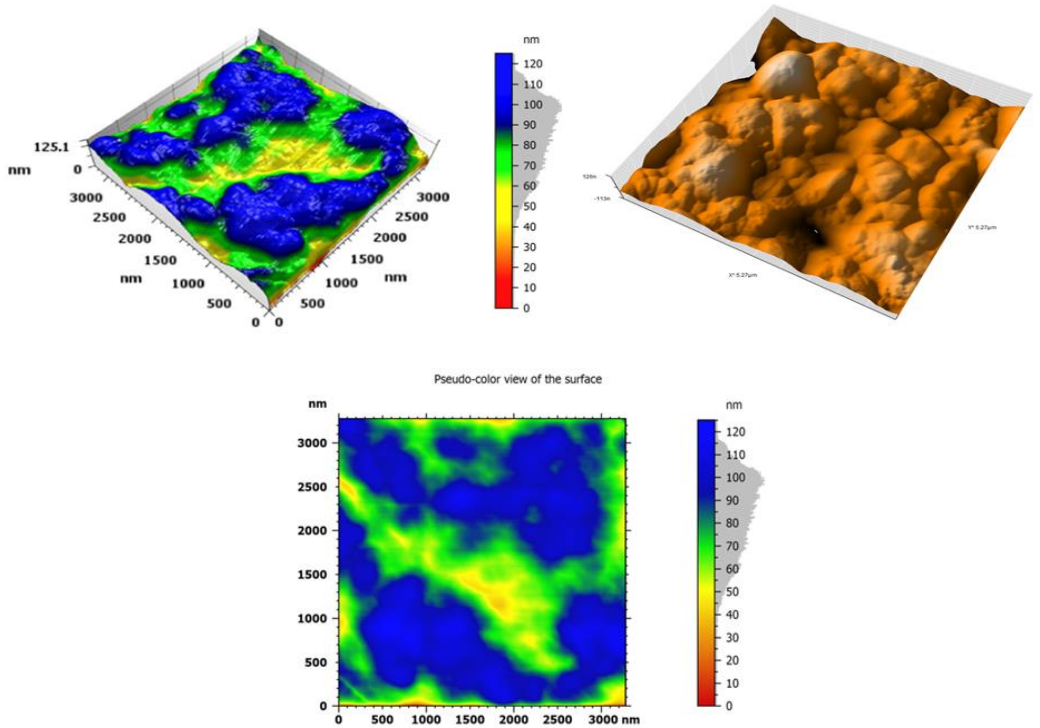

Fig. (2-c): AFM Images of $(SnO_2)_{0.92}(MnO_2)_{0.8}$ thin film.

Figure (3) shows the transmittance spectrum as a function of wavelength for the prepared thin films. It is observed from the figure (3) that the transmittance spectrum is the opposite of the absorption spectrum. The transmittance values increase with increasing wavelength for the undoped films. However, when the pure material (SnO2) is doped with different percentages (2%, 4%, 6%, 8%) of (MnO2), the transmittance decreases with increasing doping ratio, The reason for this decrease is the increased absorption resulting from the increased concentration of (MnO2). The higher concentration of (MnO2) leads to an increase in the density of localized states, making the sample more nontransparent to light [36].This results in the absorption edge extending to low energy, where the photons have sufficient energy to excite electrons from the valence band to the conduction band of the prepared films [37].

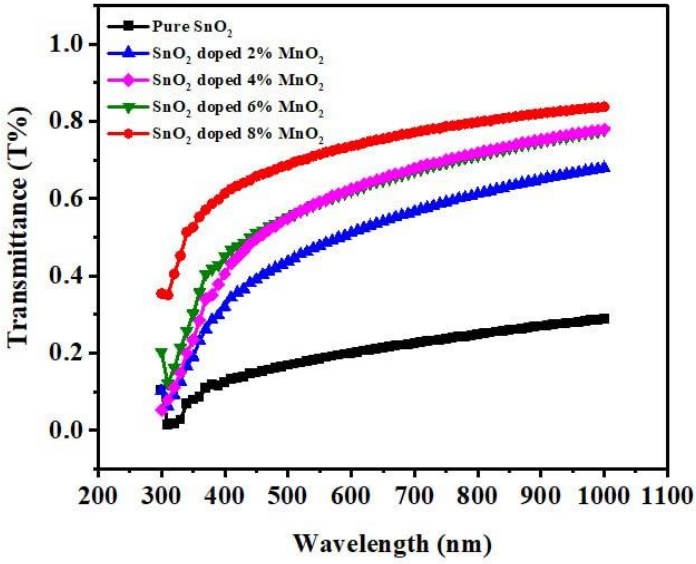

Fig. (3): Transmittance for SnO_2 doping MnO_2 films

Figure (4) shows the absorption spectrum as a function of wavelength for all prepared thin films. It is observed that the absorption value is inversely proportional to the wavelength. The absorption value reaches its minimum at a wavelength of (1100 nm) for all pure and doped films. The reason for this is that the energy of the incident photon is lower than the energy band gap, and therefore, the electron is not excited from the valence band to the conduction band. This explains the decrease in absorption with increasing wavelength [38] .When the pure material (SnO2) is doped with different percentages (2%, 4%, 6%, 8%) of (MnO2), there is a noticeable decrease in the value of processed film along with an increase in the chipping rate, and this decrease is attributed to increased absorption [38].The highest absorption value is observed at a (2%) ratio of (MnO2). This can be described by the formulation of impurity atoms and their incorporation into the crystalline structure of the prepared films. This leads to the formulation of energy levels between the energy bands, which in turn increases the absorption.

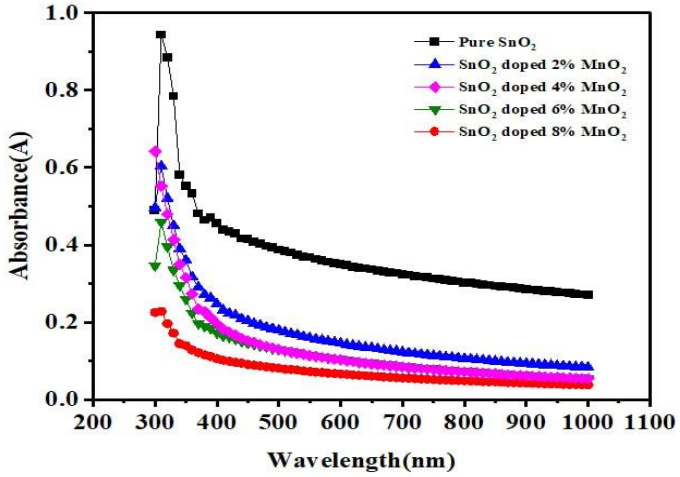

Fig. (4) : Absorbance for SnO_2 doping MnO_2 films

Figure (5) shows the reflectance values for all prepared thin films as a function of wavelength. It is observed from the figure that the reflectance values decrease with increasing wavelength. The reason for this is that the refractive index decreases with increasing wavelength, resulting in lower reflectance.

Additionally, it is noted from the figure that the reflectance values are highest when the material is pure. However, when the pure material (SnO2)is doped with different percentages (2%, 4%, 6%, 8%) of (MnO2), the reflectance values decrease. This decrease varies greatly, and the lowest reflectance value is recorded at a doping ratio of 2%. After that, the reflectance values increase for the subsequent doping ratios and then decrease again.

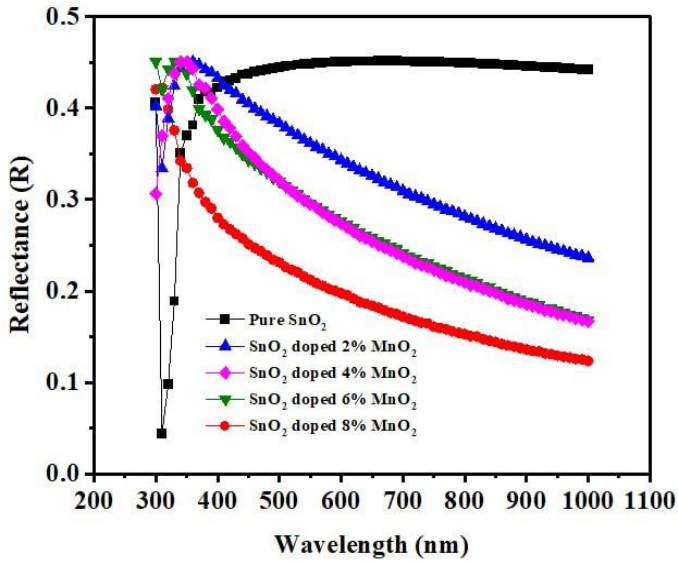

Fig.(5) : Reflectance for SnO_2 doping MnO_2 films.

The figure (6) shows the absorption coefficient as a function of incident photon energy for all prepared Films. From the figure (6) we observe that the absorption coefficient increases with increasing photon energy, and the maximum value of the absorption coefficient occurs at energy of (3-3.5) eV. This is correct for the undoped Films However, when the pure material (SnO2) is doped with different percentages (2%, 4%, 6%, 8%) of (MnO2) we observe that the absorption coefficient decreases with increasing photon energy. The lowest value of the absorption coefficient is recorded at a doping percentage of 2%, and then there is a slight increase and decrease after that .The reason for this behavior is that the doping process prevents the formulation of secondary levels within the energy gap. Consequently, the transfer of electrons with lower energy is reduced, leading to a decrease in the absorption of incident photons and, consequently, a decrease in the absorption coefficient [39].

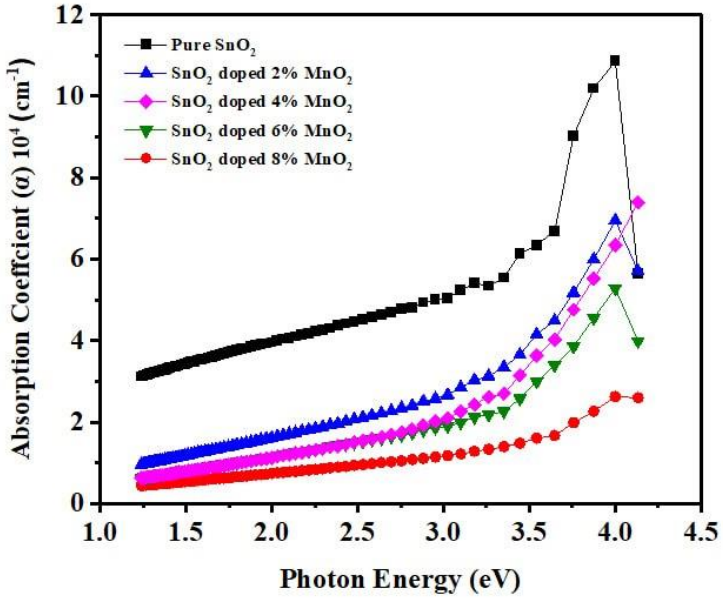

Fig. (6) : Absorption Coefficient for SnO_2 doping MnO_2 films.

The primary factor that determines the values of the optical energy gap in thin films is the crystalline structure of the membranes. The values of the energy gap are calculated using equation at the value of the constant (r = 1/2). Through the mathematical relationship between (αhv)^2 and the incident photon energy (hv) [40] , the best straight line is drawn that passes through most of the points after the basic absorption edge of the curve, intersecting the photon energy axis at point (α). This intersection point represents the value of the energy gap for the prepared membranes. Figure (7) illustrates the energy gap value of the prepared membranes as a function of the incident photon energy, It is observed that the doping process with manganese oxide (MnO2) leads to a decrease in the energy gap value, This decrease varies greatly, and it is attributed to the formation of new donor levels resulting from doping[41] . These formed levels are located within the energy gap and near the conduction band, creating bridges for the transfer of electrons with lower energy than the energy gap value of the pure membrane to the conduction band. This results in a change in the Fermi level, shifting it toward the conduction band due to the increase in the number of electronic

transitions [42].

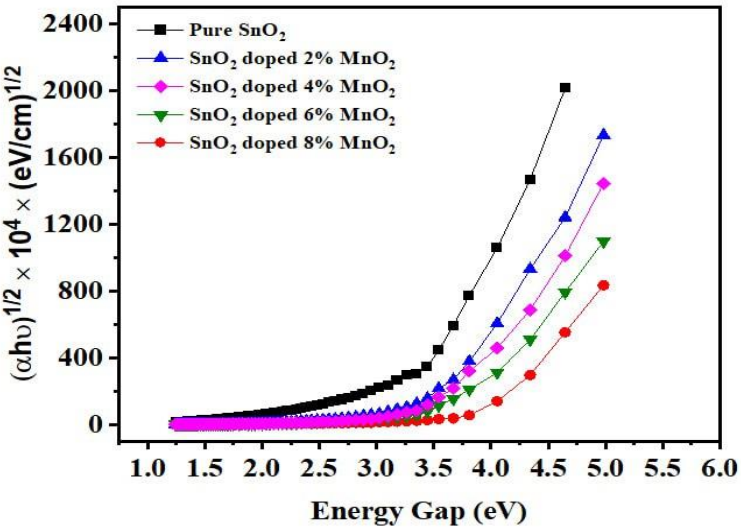

Fig. (7): Optical Energy Gap for SnO2 doping MnO2 films.

Figure (8) shows the refractive index values as a function of incident photon energy for all prepared Films. From the figure, we observe that the refractive index increases with increasing photon energy, and this behavior is similar to the reflectance spectrum for the undoped films However, when the pure material (SnO2) is doped with different raties (2%, 4%, 6%, 8%) of (MnO2)we observe that the refractive index decreases with increasing photon energy. The lowest value of the refractive index is recorded at a doping ratio 2%, and then there is a varying increase and decrease thereafter.The reason for this behavior is that the doping process prevents the addition of impurity atoms to the pure material (SnO2) This leads to a reduction in the intensity of the reflected radiation and, consequently, a decrease in the refractive index [43].

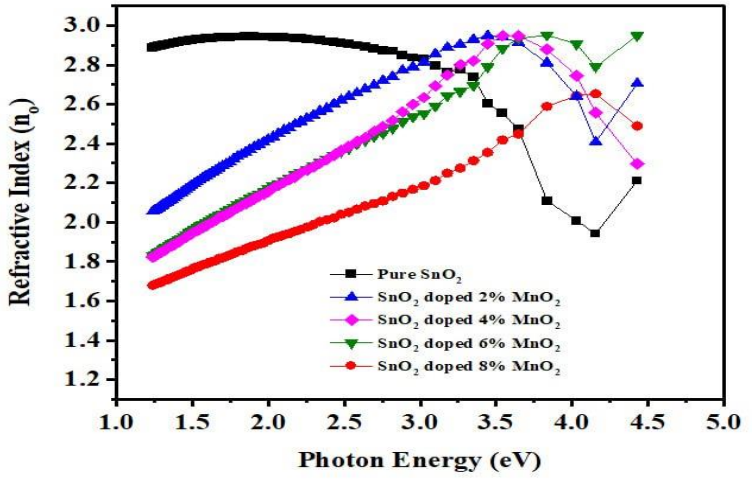

Fig. (8) : Refractive Index for SnO_2 doping MnO_2 films.

Figure (9) shows the extinction coefficient as a function of incident photon energy for all prepared Films. From the figure, we observe that the extinction coefficient decreases with increasing photon energy for all Films However, when the pure material (SnO2) is doped with different raties (2%, 4%, 6%, 8%) of (MnO2), we observe that the extinction coefficient decreases. The reason for this is that the dopant material leads to a reduction in the number of donor levels within the energy gap. These donor levels contribute to the absorption coefficient, and consequently, their decrease results in a decrease in the extinction coefficient. Therefore the doping process leads to a decrease in both the absorption coefficient and the extinction coefficient [44].

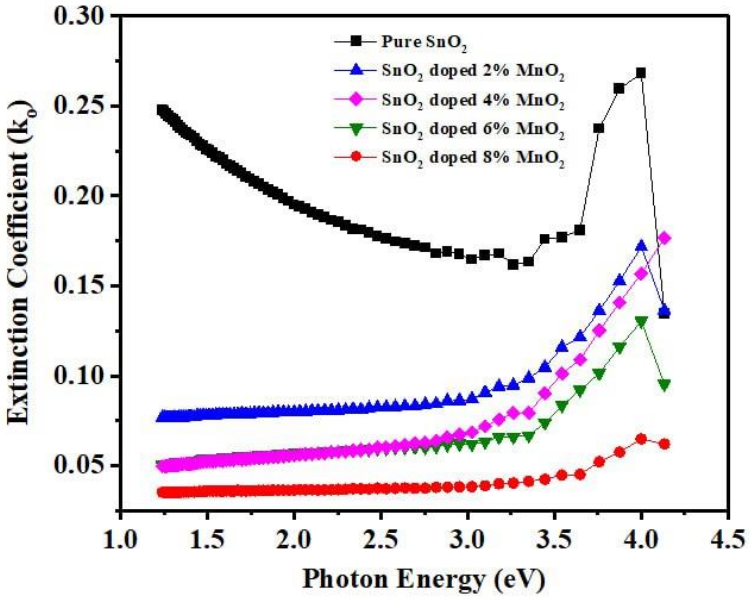

Fig. (9): Extinction Coefficient for SnO_2 doping MnO_2 films

The figure (10) shows the real dielectric constant as a function of the incident photon energy for all prepared Films. From the figure, it can be observed that the value of the real dielectric constant for pure materials decreases with increasing incident photon energy. The figure (10) also indicates that the behavior of the dielectric constant curve is similar to the behavior of the refractive index curve.When doping the pure material (SnO2) with different ratio (2%, 4%, 6%, 8%) of (MnO2) it can be noticed that the real dielectric constant increases unevenly with increasing doping ratio. The reason for this increase is the result of the high density of induced polar dipoles due to the increased doping ratio. These dipoles lead to an increase in polarization values and refractive index, thus increasing the real dielectric constant [45] .

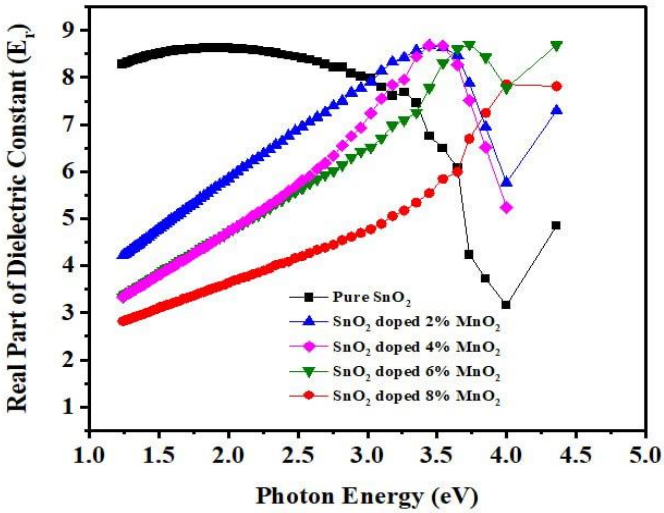

Fig. (10) : Real Part of Dielectric Constant for SnO_2 doping MnO_2 films.

The figure (11) shows the imaginary dielectric constant as a function of the incident photon energy for all prepared Films. It can be observed from the figure (11) that the imaginary dielectric constant for pure materials decreases with increasing incident photon energy.However, when doping the pure material (SnO2) with different ratio (2%, 4%, 6%, 8%) of (MnO2) it can be noticed that the imaginary dielectric constant increases with increasing doping ratio, and the increase varies unevenly. The reason for this increase is the incorporation of impurity atoms (MnO2) into the crystal structure of the pure Films (SnO2), This leads to the formulation of new energy levels within the energy gap, resulting in an increase in polarization ratio and absorbed energy, thus increasing the imaginary dielectric constant [46].

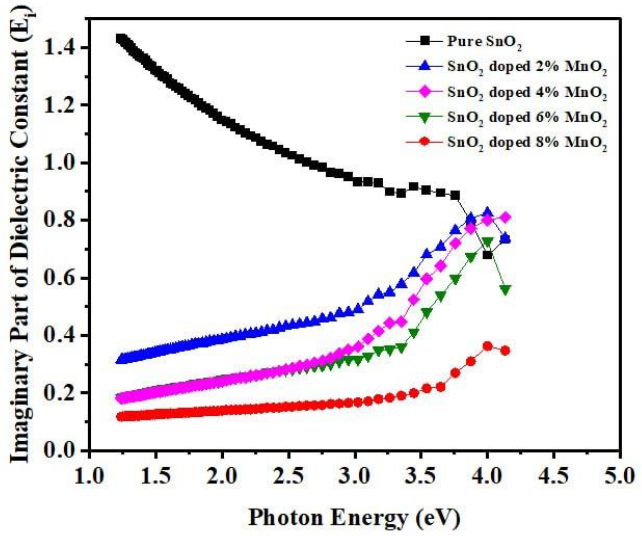

Fig. (11): Imaginary Part of Dielectric Constant for SnO_2 doping MnO_2 films.

4. Conclusions

Using the chemical spray pyrolysis technique, thin films of (SnO2) doped with (MnO2) in different ratios (2%, 4%, 6%, 8%) were prepared. Spectral analysis was performed using FE-SEM and AFM, and the optical properties of the prepared samples were investigated. The electron microscope SEM revealed that the particles form non-homogeneous agglomerates and clusters, while the surface topography by AFM showed an increase in the average surface roughness, The optical results showed that doping affects several properties. The transmittance increases with increasing wavelength, while the absorbance and reflectance are opposite to the transmittance value. The extinction coefficient, absorption coefficient, refractive index, and energy gap increase with increasing photon energy, while the real and imaginary dielectric constants decrease with increasing photon energy. The results a significant improvement in the morphology and optical properties of SnO2:MnO2 Nanostructure thin films, making them a valuable material for solar cell fabrication and sensor applications.

References

1. Kykyneshi, R., Zeng, J., & Cann, D. P. (2011). Transparent conducting oxides based on tin oxide. Handbook of transparent conductors, 171-191.
2. Abood, A. T., Hussein, O. A. A., Al-Timimi, M. H., Abdullah, M. Z., Al Aani, H. M. S., & Albanda, W. H. (2020, March). Structural and optical properties of nanocrystalline SnO2 thin films growth by electron beam evaporation. In AIP Conference Proceedings (Vol. 2213, No. 1). AIP Publishing.
3. Homada, H. T., Alia, N. M., Al-Jubourib, O. A., & Al-Timimia, M. H. (2023). Synthesis and characterization of LiCo1-xNixO2 nanoparticles by urea route as cathode for lithium-ion battery. Journal of Ovonic Research, 19(6), 783-791.
4. Čejka, J., Nachtigall, P., & Centi, G. (2018). New catalytic materials for energy and chemistry in transition. Chemical Society Reviews, 47(22), 8066-8071.
5. Al-Rikabi, H. S., Al-Timimi, M. H., & Abd, I. K. (2023, December). A review of (MgO) thin films, preparation and applications. In AIP Conference Proceedings (Vol. 2834, No. 1). AIP Publishing.
6. Bach, H., & Neuroth, N. (Eds.). (1998). The properties of optical glass. Springer Science & Business Media.
7. Gao, T., Glerup, M., Krumeich, F., Nesper, R., Fjellvåg, H., & Norby, P. (2008). Microstructures and spectroscopic properties of cryptomelane-type manganese dioxide nanofibers. The Journal of Physical Chemistry C, 112(34), 13134-13140.
8. Najafpour, M. M., Renger, G., Hołynska, M., Moghaddam, A. N., Aro, E. M., Carpentier, R., ... & Allakhverdiev, S. I. (2016). Manganese compounds as water-oxidizing catalysts: from the natural water-oxidizing complex to nanosized manganese oxide structures. Chemical reviews, 116(5), 2886-2936.
9. Wang, S., Li, L., Sun, Z., Ji, C., Liu, S., Wu, Z., ... & Luo, J. (2017). A semi-conductive organic–inorganic hybrid emits pure white light with an ultrahigh color rendering index. Journal of Materials Chemistry C, 5(19), 4731-4735.
10. Ryu, I., Kim, G., Park, D., & Yim, S. (2015). Ethanedithiol-treated manganese oxide nanoparticles for rapidly responsive and transparent supercapacitors. Journal of Power Sources, 297, 98-104.
11. Saeed, F. R., Al-Timimi, M. H. A. A., Al-Banda, W. H. A., Abdullah, M. Z., Stamatin, I., Voinea, S., ... & Balan, A. E. (2018). THERMAL PROPERTIES OF PARAFFIN/NANO-MAGNETITETREVORITE PHASE CHANGE MATERIALS. Journal of Ovonic Research,

14(5).
12. Abdullah, M. Z., Hasan, H. M., Al-Timimi, M. H., Albanda, W. H., Alhussainy, M. K., & Dumitru, M. (2019). Preparation And Characterization Of Carbon Doped Lithium Iron Phosphate Composite As Cathode For Rechargable Battery. Journal of Ovonic Research Vol, 15(3), 199-204.
13. Goyal, R., Singh, O., Agrawal, A., Samanta, C., & Sarkar, B. (2022). Advantages and limitations of catalytic oxidation with hydrogen peroxide: from bulk chemicals to lab scale process. Catalysis Reviews, 64(2), 229-285.
14. Aelawi, W. A., Alptekin, S., & Al-Timimi, M. H. (2023). Structural, optical, and electrical properties of nanocrystalline CdS1− X CuSX thin films. Indian Journal of Physics, 97(13), 3949-3956.
15. Al-Timimi, M. H., Albanda, W. H., & Abdullah, M. Z. (2023). Influence of Thickness on Some Physical Characterization for Nanostructured MgO Thin Films. East European Journal of Physics, (2), 173-181.
16. Catania, F., de Souza Oliveira, H., Lugoda, P., Cantarella, G., & Münzenrieder, N. (2022). Thin-film electronics on active substrates: review of materials, technologies and applications. Journal of Physics D: Applied Physics, 55(32), 323002.
17. Kannan, N., & Vakeesan, D. (2016). Solar energy for future world:-A review. Renewable and sustainable energy reviews, 62, 1092-1105.
18. Al-Rikabi, H. S., Al-Timimi, M. H., & Albanda, W. H. (2022). Morphological and optical properties of MgO1-xZnSx thin films. Digest Journal of Nanomaterials & Biostructures (DJNB), 17(3).
19. Kim, J., Kumar, R., Bandodkar, A. J., & Wang, J. (2017). Advanced materials for printed wearable electrochemical devices: A review. Advanced Electronic Materials, 3(1), 1600260.
20. Saeed, M. H., Al-Timimi, M. H., & Hussein, O. A. A. (2021). Structural, morphological and optical characterization of nanocrystalline WO3 thin films. Digest Journal of Nanomaterials and Biostructures, 16(2), 563-569.
21. Ali, S. M., Lateef, R. A., & AL-TIMIMI, M. H. (2023). Antimicrobial Activity of Copper Oxide Nanoparticles on Multidrug Resistant Bacteria MDR and C. albicans. Academic Science Journal, 1(1), 39-74.
22. Safarian, J., & Engh, T. A. (2013). Vacuum evaporation of pure metals. Metallurgical and Materials Transactions A, 44(2), 747-753.
23. Gosiewski, K., Pawlaczyk, A., Warmuzinski, K., & Jaschik, M. (2009). A study on thermal combustion of lean methane–air mixtures: Simplified reaction mechanism and kinetic equations. Chemical Engineering Journal, 154(1-3), 9-16.
24. Lokhande, C. D. (1991). Chemical deposition of metal chalcogenide thin films. Materials Chemistry and Physics, 27(1), 1-43.
25. Fambri, L., & Migliaresi, C. (2022). Crystallization and thermal properties. Poly (Lactic Acid) Synthesis, Structures, Properties, Processing, Applications, and End of Life, 135-151.
26. Jassim, N. M., Khodair, Z. T., Diwan, M. H., & Al Timimi, M. H. (2019). Preparation, morphology and study of some nonlinear optical properties of hybrid cadmium sulfied coated gold nanowires. Journal of Ovonic Research, 15(4), 221-226.
27. Dedova, T. (2007). Chemical spray pyrolysis deposition of zinc sulfide thin films and zinc oxide nanostructured layers. Tallinn, Estonia: Tallinn University of Technology.
28. Guild, C., Biswas, S., Meng, Y., Jafari, T., Gaffney, A. M., & Suib, S. L. (2014). Perspectives of spray pyrolysis for facile synthesis of catalysts and thin films: An introduction and summary of recent directions. Catalysis Today, 238, 87-94.
29. Gandhi, T. I., Babu, R. R., Ramamurthi, K., & Arivanandhan, M. (2016). Effect of Mn doping on the electrical and optical properties of SnO2 thin films deposited by chemical spray pyrolysis technique. Thin Solid Films, 598, 195-203.

30. Fraas, L. M., & Partain, L. D. (2010). Solar cells and their applications. John Wiley & Sons.
31. Cerchier, P., Dabalà, M., & Brunelli, K. (2017). Synthesis of SnO 2 and Ag Nanoparticles from Electronic Wastes with the Assistance of Ultrasound and Microwaves. JOM, 69, 1583-1588.
32. Vadivel, S., & Rajarajan, G. (2015). Effect of Mg doping on structural, optical and photocatalytic activity of SnO 2 nanostructure thin films. Journal of Materials Science: Materials in Electronics, 26, 3155-3162.
33. Hammoodi, F. G., Shuihab, A. A., & Ebrahiem, S. A. (2021, July). Studying The Topographic and Morphology Structure of CdO: In Thin Films. In Journal of Physics: Conference Series (Vol. 1963, No. 1, p. 012121). IOP Publishing.
34. Al-Rikabi, H. S., Al-Timimi, M. H., Abed, A. H., & ALBANDA, W. (2022). Surface Topography and Optical Properties for (MgOx-1ZnSx) Thin Films Prepared by Chemical Spray Pyrolysis. Academic Science Journal, 18(4).
35. Chiad, S. S., Habubi, N. F., Abass, W. H., & Abdul-Allah, M. H. (2016). Effect of thickness on the optical and dispersion parameters of Cd0. 4Se0. 6 thin films. Journal of Optoelectronics and Advanced Materials, 18(9-10), 822-826.
36. F. T. Ibrahim, "Characterization of Pulsed-Laser Deposited CuODoped MgO Thin Films for Gas Sensing Applications", IraqiJournal of Applied Physics, Vol. 13, No. 3, 2017.
37. Al-Mgrs, S. S. H., Al-Timimi, M. H., Abdullah, M. Z., & Al-Banda, W. H. (2023, March). Structural and optical characterizations of synthesized CMC/PVP-SnO2 nano composites. In AIP Conference Proceedings (Vol. 2475, No. 1). AIP Publishing.
38. Hammoodi, F. G., Shuihab, A. A., & Ebrahiem, S. A. (2022, November). Synthesis and studying of some properties of CdO: in thin films. In AIP Conference Proceedings (Vol. 2394, No. 1). AIP Publishing.
39. E. Parvizi, R. Tayebee, and E. Koushki, "Mg-doped ZnO and Zndoped MgO semiconductor nanoparticles; synthesis and catalytic,optical and electro-optical characterization", Semiconductors, Vol.53, No. 13, pp. 1769-1783, 2019.
40. Abdullal, M. H., Jaseen, R. A., & Resan, A. H. (2011). Annealing effect on the optical energy gap of (CdTe) thin films. J. Pure Sciences, 7(3), 205-213.
41. O. N. Ogada, "Effect of concentration of reactants and depositiontemperature on the optical properties of iron-doped cadmiumstannate thin films deposited on glass substrates by spray pyrolysis",Maseno University, 2019.
42. Abbas, M. M., Abdallah, M. H., & Alwan, T. J. (2014). Synthesis and Optical Characterization of Nickel Doped Poly Vinyl Alcohol Films. SOP Transactions on Physical Chemistry, 1(2), 1-9.
43. Abdul-Allah, M. H., Salman, S. A., & Abbas, W. H. (2014). Annealing effect on the structural and optical properties of (CuO)(Fe2O3) x thin films obtained by chemical spray pyrolysis. Journal of Thi-Qar Science, 5(1).
44. Abdul-Allah, M. H., Chiad, S. S., & Habubi, N. F. (2010). The effect of Iron chromate on the optical properties of PMMA films. Diyala journal for pure sciences, 6(2), 161-169.
45. Hussein, H. M., & Al-Timimi, M. H. (2022). Preparation and Study Some Physical Properties of (CMC/PAA: MgO) Nano Composites. Eurasian Journal of Physics, Chemistry and Mathematics, 8, 47-55.
46. Hassan, N. A., Albanda, W. H., & Al-Timimi, M. H. (2023). Effect of ZnS and CdS on Some Physical Properties of MgO Films. East European Journal of Physics, (3), 296-302.